Non-invasive optical mapping of the piglet brain in real time

Sergio Fantini, Maria Angela Franceschini and Enrico Gratton

Laboratory for Fluorescence Dynamics, Department of Physics,
University of Illinois at Urbana-Champaign, 1110 West Green Street, Urbana, IL 61801

fantini@uiuc.edu
http://www.physics.uiuc.edu/groups/fluorescence/staff/fantini/

Dennis Hueber

ISS, Incorporated, 2604 North Mattis Avenue, Champaign, IL 61821

Warren Rosenfeld and Dev Maulik

Departments of Obstetrics/Gynecology & Pediatrics, Winthrop University Hospital
State University of New York, Stony Brook School of Medicine, 259 First Street, Mineola, NY 11501

Phillip G. Stubblefield

Department of Obstetrics and Gynecology
Boston University School of Medicine, 1 Boston Medical Center Place, Boston, MA 02118

Miljan R. Stankovic

Departments of Obstetrics/Gynecology & Pediatrics, Winthrop University Hospital
State University of New York, Stony Brook School of Medicine, 259 First Street, Mineola, NY 1150

Department of Obstetrics and Gynecology
Boston University School of Medicine, 1 Boston Medical Center Place, Boston, MA 02118

Abstract: We have performed non-invasive, real-time optical mapping of the piglet brain during a subcortical injection of autologous blood. The time resolution of the optical maps is 192 ms, thus allowing us to generate a real-time video of the growing subcortical hematoma. The increased absorption at the site of blood injection is accompanied by a decreased absorption at the contralateral brain side. This contralateral decrease in the optical absorption and the corresponding time traces of the cerebral hemoglobin parameters are consistent with a reduced cerebral blood flow caused by the increased intracranial pressure.

OCIS codes: (170.3880) Medical and biological imaging; (170.3890) Medical optics instrumentation; (170.5280) Photon migration

References and links

1. See papers in *Optical tomography and spectroscopy of tissue III*, B. Chance, R. R. Alfano and B. J. Tromberg, Proc. SPIE **3597** (1999).
2. J. C. Hebden and R. A. Kruger, "Transillumination imaging performance: Spatial resolution simulation studies," Med. Phys. **17**, 41-47 (1990).
3. G. Mitic, J. Kölzer, J. Otto, E. Plies, G. Sölkner and W. Zinth, "Time-gated transillumination of biological tissues and tissuelike phantoms," Appl. Opt. **33**, 6699-6710 (1994).

#9266 - $15.00 US Received March 09, 1999; Revised April 07, 1999

4. D. T. Delpy, M. Cope, P. van der Zee, S. Arridge, S. Wray and J. Wyatt, "Estimation of optical pathlength through tissue from direct time of flight measurement," Phys. Med. Biol. **33**, 1433-1442 (1988).
5. S. Fantini, D. Hueber, M. A. Franceschini, E. Gratton, W. Rosenfeld, P. G. Stubblefield, D. Maulik and M. R. Stankovic, "Non-invasive optical monitoring of the newborn piglet brain using continuous-wave and frequency-domain spectroscopy," Phys. Med. Biol. (*submitted*).
6. S. Fantini, M. A. Franceschini and E. Gratton, "Semi-infinite-geometry boundary problem for light migration in highly scattering media: a frequency-domain study in the diffusion approximation," J. Opt. Soc. Am. B **11**, 2128-2138 (1994).
7. M. A. Franceschini, S. Fantini, L. A. Paunescu, J. S. Maier and E. Gratton, "Influence of a superficial layer in the quantitative spectroscopic study of strongly scattering media," Appl. Opt. **37**, 7447-7458 (1998).
8. E. M. Sevick, B. Chance, J. Leigh, S. Nioka and M. Maris, "Quantitation of time- and frequency-resolved optical spectra for the determination of tissue oxygenation," Anal. Biochem. **195**, 330-351 (1991).
9. M. A. Franceschini, S. Fantini, A. E. Cerussi, B. Barbieri, B. Chance and E. Gratton, "Quantitative spectroscopic determination of hemoglobin concentration and saturation in a turbid medium: Analysis of the effect of water absorption," J. Biomed. Opt. **2**, 147-153 (1997).
10. M. R. Stankovic, D. Hueber, D. Maulik, P. G. Stubblefield, W. Rosenfeld, E. Gratton, M. A. Franceschini and S. Fantini, "Real-time optical imaging and spectroscopy of brain ischemia and hemorrhage," in Optical tomography and spectroscopy of tissue III, B. Chance, R. R. Alfano and B. Tromberg, eds., Proc. SPIE **3597**, (*in press*).
11. A. Maki, Y. Yamashita, Y. Ito, E. Watanabe, Y. Mayanagi and H. Koizumi, "Spatial and temporal analysis of human motor activity using noninvasive NIR topography," Med. Phys. **22**, 1997-2005 (1995).
12. B. Chance, E. Anday, S. Nioka, S. Zhou, L. Hong, K. Worden, C. Li, T. Murray, Y. Ovetsky, D. Pidikiti and R. Thomas, "A novel method for fast imaging of brain function, non-invasively, with light," Opt. Express **2**, 411-423 (1998).
13. R. M. Danen, Y. Wang, X. D. Li, W. S. Thayer and A. G. Yodh, "Regional imager for low-resolution functional imaging of the brain with diffusing near-infrared light," Photochem. Photobiol. **67**, 33-40 (1998).
14. S. R. Hintz, D. A. Benaron, J. P. van Houten, J. L. Duckworth, F. W. H. Liu, S. D. Spilman, D. K. Stevenson and W.-F. Cheong, "Stationary headband for clinical time-of-flight optical imaging at the bedside," Photochem. Photobiol. **68**, 361-369 (1998).
15. S. R. Hintz, W.-F. Cheong, J. P. van Houten, D. K. Stevenson and D. A. Benaron, "Bedside imaging of intracranial hemorrhage in the neonate using light: Comparison with ultrasound, computed tomography, and magnetic resonance imaging," Pediatr. Res. **45**, 54-59 (1999).
16. J. P. van Houten, D. A. Benaron, S. Spilman and D. K. Stevenson, "Imaging brain injury using time-resolved near infrared light scanning," Pediatr. Res. **39**, 470-476 (1996).
17. Y. Shinohara, M. Haida, N. Shinohara, F. Kawaguchi, Y. Itoh and H. Koizumi, "Towards near-infrared imaging of the brain," Adv. Exp. Med. Biol. **413**, 85-89 (1997).
18. C. Hirth, K. Villringer, A. Thiel, J. Bernarding, W. Mühlnickl, H. Obrig, U. Dirnagl and A. Villringer, "Towards brain mapping combining near-infrared spectroscopy and high resolution 3D MRI," Adv. Exp. Med. Biol. **413**, 139-147 (1997).

1. Introduction

Near-infrared light penetrates deeply into most biological tissues, thus providing a potentially effective probe for non-invasive tissue imaging at a macroscopic level [1]. The spatial resolution of optical imaging is limited by the diffusive character of light propagation inside tissues [2,3]. However, the optical approach shows three features that render it a unique imaging modality: (1) optical inhomogeneities in the tissue may be visualized with high contrast; (2) real-time imaging is feasible; (3) quantitative information on the hemoglobin concentration and saturation can be achieved. In this article, we report results on an animal model that show all three of these features of the optical technique.

2. Methods

We have investigated two newborn piglets, one for near-infrared imaging and one for quantitative optical spectroscopy. The piglets were anesthetized (propofol and sodium pentobarbital) and ventilated (Bear CUB Infant Ventilator, Bear Medical Systems, Inc., Riverside, CA), and a catheter was inserted in the abdominal aorta for continuous mean arterial blood pressure measurement (Hewlett Packard 78353B, USA). A pulse oximeter (Nellcor PM-1000, Nellcor, Inc., Hayward, CA) was attached to the tail of the piglet to monitor the heart rate. In the imaging experiment, we injected 2 cc of autologous venous blood in the brain, at a depth of 1.2 cm from the skin to produce a subcortical hematoma. The injection site on the piglet head (left anterior quadrant) is shown in Fig. 1(a). The blood

#9266 - $15.00 US Received March 09, 1999; Revised April 07, 1999

was injected continuously, over a time of about 30 s. The blood injection followed a 0.3 cc injection (lasting about 8 s) of an optically clear physiological solution (saline) that was used to fill up the tubing connecting the syringe to the needle. In the spectroscopy experiment, we injected 2 cc of saline over a period of about 30 s in order to investigate the effect of an increased intracranial pressure. The injection site (Fig. 1(c)) is the same as for the imaging experiment, and the spectroscopy probe is located on the opposite (contralateral) brain side.

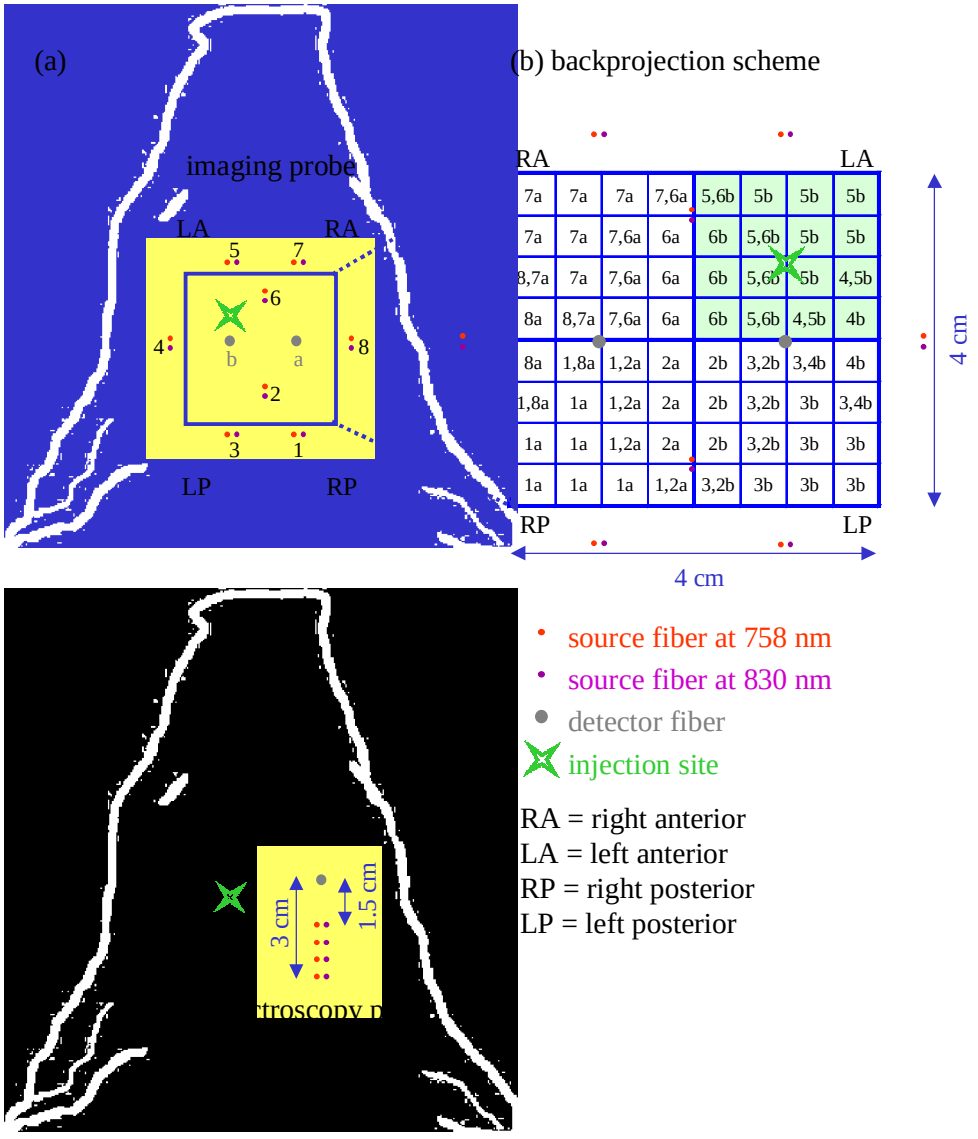

Fig. 1. Geometrical arrangement of the source fibers (at 758 and 830 nm) and the detector fibers in the imaging probe (panel (a)) and in the spectroscopy probe (panel (c)) on the piglet head. The injection site at the piglet head is also shown. Panel (b) gives the 2-D backprojection scheme used to generate the optical maps. Pixel size is 0.5×0.5 cm^2. The numbers in each pixel (1-8) refer to a source location, while the letters (a,b) refer to a detector location (see panel (a)). For instance, the pixels labeled 8a are determined by the readings of the source-detector pair 8a, whereas the pixels labeled 7,6a are determined by the average of the readings of source-detector pairs 6a and 7a. Note the exchange of the right and left sides in panel (b) (backprojected optical image of the brain) with respect to panels (a) and (c) (top view of the piglet head).

#9266 - $15.00 US
Received March 09, 1999; Revised April 07, 1999

For the optical measurements, we have used a dual-channel frequency-domain tissue spectrometer (Model No. 96208, ISS, Inc., Champaign, IL) operating at a modulation frequency of 110 MHz, and at two near-infrared wavelengths (758 and 830 nm). The sixteen laser diodes (eight at 758 nm, and eight at 830 nm) are electronically multiplexed to turn them on and off in sequence every 12 ms (for imaging) or 20 ms (for spectroscopy). Each laser diode is coupled to an optical fiber 400 μm in core diameter, while each of the two photomultiplier tube detectors is coupled to a fiber-bundle 3 mm in internal diameter. The source and detector fibers are placed in contact with the skin of the piglet head, according to the configurations shown in Fig. 1(a) (for spatial mapping) and Fig. 1(c) (for local spectroscopy). The acquisition time in the mapping experiment is 192 ms (16 diodes×12 ms/diode) per image, while in the spectroscopy experiment it is 160 ms (8 diodes×20 ms/diode) per data point.

The optical maps are computed by backprojecting the absorption changes measured at the various source-detector pairs. The backprojection scheme, aiming at a quadrant resolution, is illustrated in Fig. 1(b). For each 0.5×0.5 cm^2 pixel, Fig. 1(b) indicates the source detector pair(s) whose readings have been considered to yield the corresponding pixel value. The pixel values have been linearly interpolated to produce the final optical maps. The absorption changes are obtained from the intensity measurements according to the differential pathlength factor (DPF) method [4]. The value of the DPF for the piglet brain was not taken from the literature, but it was obtained from the spectroscopy experiment by using the diffusion theory expression that relates the DPF to μ_a and μ_s' in a semi-infinite geometry [5]. At 830 nm, and in the range of source-detector distances featured in the imaging probe (1.8-2.5 cm), we found values of the DPF ranging from 5.3 to 5.7. Our optical maps are not quantitatively accurate because of the use of a straightforward backprojection scheme, and because of the high absorption coefficient (~5 cm^{-1}) of the injected blood.

The spectroscopy measurements have been performed (1) to determine the differential pathlength factor (DPF) for the piglet brain, and (2) to quantitatively measure the hemodynamics on the side contralateral to the subcortical injection. The frequency-domain data (amplitude and phase) collected by the spectroscopy probe (Fig. 1(c)) are analyzed with the multi-distance method to yield the absolute values of the cerebral μ_a and μ_s' [6]. The range of source-detector separations is 1.5-3.0 cm. This multi-distance method is based on diffusion theory, and it assumes a uniform, semi-infinite medium. The influence of the inhomogeneity resulting from the presence of the scalp-skull layer (~4 mm thick) is considered to be negligible on the basis of an experimental study conducted on two-layered, tissue-like phantoms [7]. The concentrations of oxy-hemoglobin ($[HbO_2]$) and deoxy-hemoglobin ([Hb]) are obtained from μ_a at two wavelengths, assuming that hemoglobin is the dominant absorbing species in the near-infrared [8], and by taking into account the small contribution of water absorption [9]. The cerebral hemoglobin saturation Y is given by $[HbO_2]/([HbO_2]+[Hb])$.

3. Results and discussion

Two representative optical maps of the piglet brain at 830 nm are shown in Figs. 2(a) (baseline) and (b) (at the time of 2 cc injected blood). The baseline map is flat by definition, because we are showing absorption changes from the initial values. The map of Fig. 2(b) shows the evident increase in the effective absorption of the left anterior (LA) quadrant (by about 0.07 cm^{-1}), as a result of the subcortical blood injection.

#9266 - $15.00 US Received March 09, 1999; Revised April 07, 1999

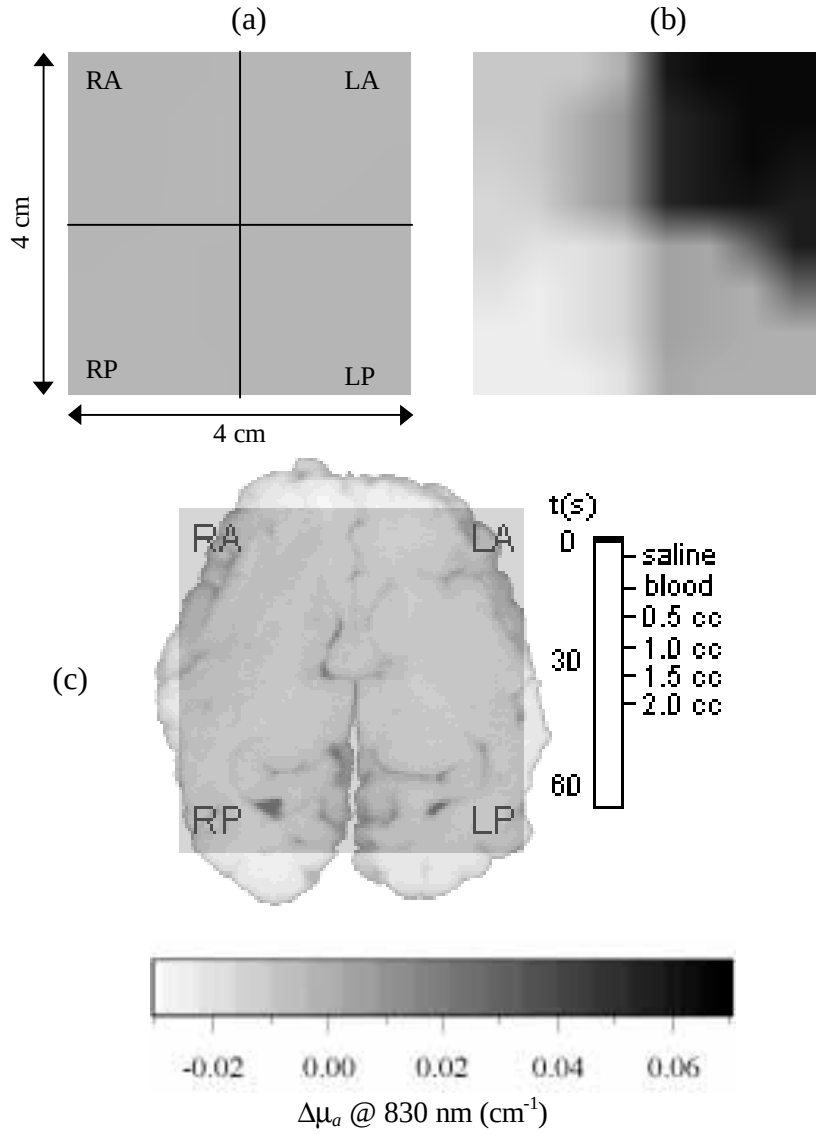

Fig. 2. (a) Baseline optical map of the piglet brain showing the right anterior (RA), left anterior (LA), right posterior (RP), and left posterior (LP) quadrants. (b) Optical map showing the changes in the effective absorption coefficient ($\Delta\mu_a$) at 830 nm caused by a subcortical injection of 2 cc of autologous blood in the left anterior (LA) quadrant. (c) Initial frame of a real-time video of the subcortical hemorrhage as optically measured non-invasively (brain_map.mov: 777 kB). The superimposed photograph of a slice of the piglet brain gives a qualitative spatial reference for the optical map. The temporal bar indicates the succession of the events during the video. Saline: start of the 0.3 cc saline injection. Blood: start of the continuous injection of 2 cc of autologous blood (the amount of injected blood is updated every 0.5 cc). The quantitative gray-level bar for $\Delta\mu_a$ refers to all three panels.

In a different experiment, we have found that the optical effect of the hemorrhage increases linearly with its surface area rather than with its volume [10]. This result indicates that the cerebral hemorrhage acts as a perfect absorber, so that the level of oxygenation of the injected blood does not affect the optical image. For this reason, the optical maps at the two wavelengths are similar, and we only show the images at 830 nm. By contrast, in the right

#9266 - $15.00 US
Received March 09, 1999; Revised April 07, 1999

posterior (RP) quadrant, which is contralateral to the injection site, we observe a decrease in the cerebral absorption. We believe that this lower absorption is due to a decreased cerebral blood flow caused by the increased intracranial pressure associated with the subcortical injection. This phenomenon is studied in more detail in the spectroscopy experiment. Figure 2(c) is the first frame of the real-time video of the subcortical injection. This video is made of about 330 frames, each corresponding to an optical map acquired in 192 ms. In the video, especially during the initial phase of the subcortical injection, one can observe the absorption fluctuations associated with the arterial pulsation (having a frequency of 1.88 Hz, or a period of 0.53 s, before the injection). As the saline injection is started, the absorption decreases both at the injection site (because the saline is optically clear), and, with a delay of a few seconds, at the contralateral side (because of the reduced cerebral blood flow associated with the increased intracranial pressure). As the blood injection is started, the absorption rapidly increases at the injection site, while it keeps decreasing at the contralateral side. Finally, after the end of the injection, the contralateral side starts recovering as a result of the reperfusion determined by the increased mean arterial blood pressure (that raised to 81 mmHg from a baseline value, before injection, of 73 mmHg), and by the increased heart rate (30 s after the end of the injection, the heart rate went up to 2.5 Hz, or 0.4 s period).

The hemodynamic response to the increase in the intracranial pressure is investigated in more detail, in the second piglet, with the spectroscopy probe located on the side contralateral to the injection site. We recall that in this case we have injected 2 cc of saline instead of 2 cc of blood. Figure 3(a) shows the cerebral oxy-hemoglobin ($[HbO_2]$), deoxy-hemoglobin ([Hb]), and total hemoglobin (THC) concentrations before, during, and after the saline injection. During the saline injection, we observed an overall decrease in THC, determined by a decrease in $[HbO_2]$ and an increase in [Hb]. This pattern is consistent with a reduction in the cerebral blood flow during the injection. After the end of the injection, the cerebral blood flow is restored through an overshoot in the $[HbO_2]$ and in the THC. The cerebral saturation, which is shown in Fig. 3(b), decreases from a baseline value of about 59% down to a minimum value of about 42% at the end of the injection.

The tip of the needle used for the blood injection was placed at a depth of 1.2 cm from the skin. Since the outer skin/scalp/skull layer measured 0.4 cm, the injection site is 0.8 cm inside the brain. At the initial stage of the injection, the blood accumulates around the tip of the needle. Therefore, we have used the initial increase in the absorption to estimate the sensitivity of the optical measurement to a hemorrhage at a depth of 1.2 cm. We found that 0.04 cc of blood (about 0.4 cm in diameter) at this depth gives an increase in the optical absorption larger than three standard deviations during baseline. This result shows that it is possible to non-invasively, optically detect a 0.04 cc hematoma at a depth of 1.2 cm inside the piglet head. After the piglet was sacrificed, we have verified the location and the size of the subcortical hemorrhage induced by the blood injection. We found that the hemorrhage had a linear size ranging from 1 to 2 cm in the three spatial dimensions, and had a minimum depth of about 0.6 cm (i.e. 0.2 cm inside the brain).

4. Conclusion

We have reported a real-time optical mapping of the piglet brain during experimental hemorrhage induced by a subcortical injection of autologous blood. The novelty of our approach is the fast acquisition time of the optical maps, namely 192 ms, which allowed us to produce a real-time video of the temporal evolution of the subcortical hemorrhage. Other groups have reported longer acquisition times in non-invasive optical brain imaging of 5 s [11], <30 s [12], 2.5 min [13], several hours [14,15], 1-3 days [16], and not-better-quantified “slow data acquisition rate” [17] and “long measurement times” [18]. Our fast acquisition rate provides a tool to investigate the spatial distribution of the arterial pulsation, which may result in a practical approach to assessing tissue viability in human subjects.

#9266 - $15.00 US Received March 09, 1999; Revised April 07, 1999

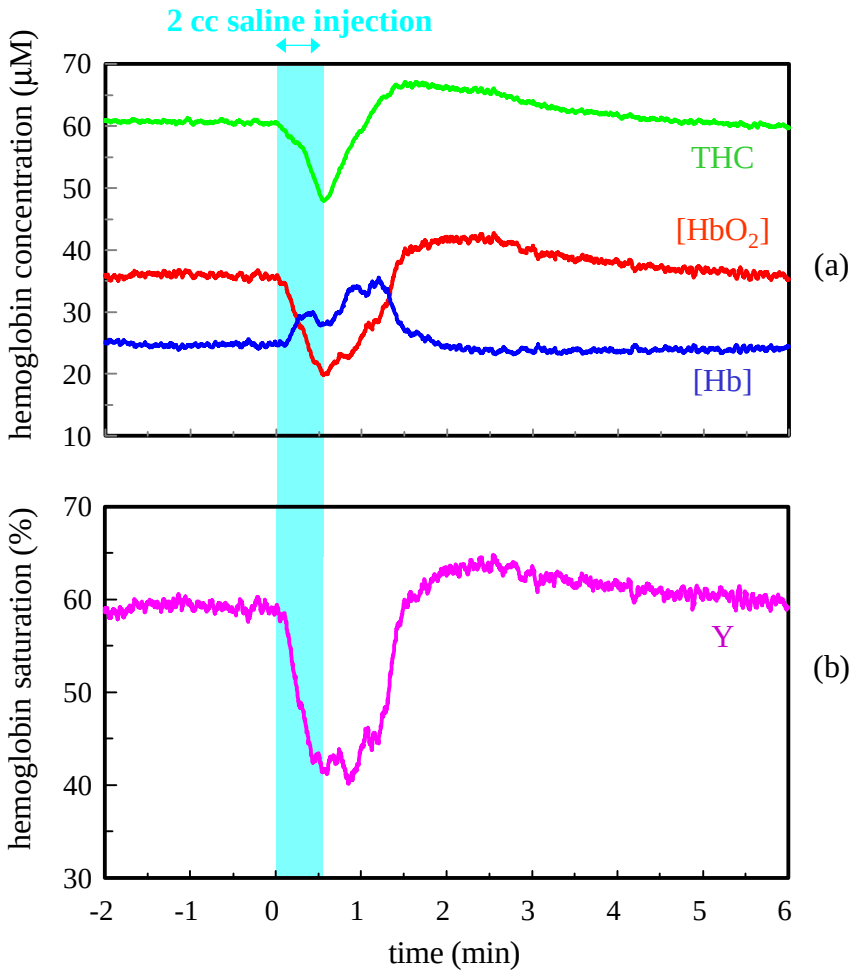

Fig. 3. Time traces of cerebral hemoglobin parameters before, during, and after a 2 cc subcortical saline injection in the contralateral side of the brain (see Fig. 1(c) for the position of the optical probe relative to the injection site). (a) oxy-hemoglobin ([HbO_2]), deoxy-hemoglobin ([Hb]), and total hemoglobin (THC) concentrations. (b) Cerebral hemoglobin saturation (*Y*).

Acknowledgments

We thank Jean Handel, Darrin Chester, Pauline Bitteto, and Patricia Johnson for their technical assistance. This research is supported in part by the US National Institutes of Health (NIH) Grant No. CA57032, and by Whitaker-NIH Grant No. RR10966.